

Structure and properties of novel cellulose-based fibers spun from aqueous NaOH solvent under various drawing conditions

Wencong Wang · Faxue Li · Jianyong Yu ·
Patrick Navard · Tatiana Budtova

Received: 30 November 2014 / Accepted: 8 January 2015 / Published online: 18 January 2015
© Springer Science+Business Media Dordrecht 2015

Abstract Hydroxyethyl cellulose (HEC) fibers with low degree of substitution were prepared by wet spinning of solutions in 8 wt% aqueous NaOH solvent. The spinning solution had a classical shear-thinning behavior and a good stability towards gelation according to its rheological behavior. The influence of drawing conditions on the structural characteristics and tensile properties of the resultant HEC fibers was investigated using synchrotron X-ray measurements, scanning electron microscope and tensile tests. HEC fibers exhibited circular cross-sections with soft and deformable surface layer as well as relatively uniform and dense inner structure. Regardless of the different jet stretch or post-drawing conditions, most of the structural features and the tensile properties of HEC fibers were improved as the

drawing ratio increased. Post-drawing was confirmed to be the key factor in controlling the fiber structure and tensile properties due to plastic deformation. Excellent tensile properties were found for HEC fibers prepared at relatively low jet ratio associated with high post-drawing ratio.

Keywords Hydroxyethyl cellulose (HEC) fibers · Drawing ratio · Structural characteristics · Tensile properties

Introduction

Regenerated cellulose fibers, inheriting comfort properties from natural cotton fibers, have attracted enormous attention and research enthusiasm in recent years. So far, the conventional viscose process is still the leading route to manufacture regenerated cellulose fibers considering the cost and quality of the fibers. The process is based on the dissolution of cellulose xanthogenate in NaOH aqueous solution followed by wet spinning into a coagulation bath composed of $H_2SO_4/Na_2SO_4/ZnSO_4$. However, the viscose industry faces a tremendous challenge with regard to the accompanying hazardous byproducts (CS_2 , H_2S and heavy metals) (Philipp 1993). Lyocell route is, for the time being, the main alternative for viscose technology. Fibers are prepared by a direct dissolution of cellulose in non-toxic solvent *N*-methyl-morpholine-

W. Wang · F. Li (✉)

College of Textiles, The Key Lab of Textile Science and Technology Ministry of Education, Donghua University, Shanghai 201620, China
e-mail: fxlee@dhu.edu.cn

J. Yu (✉)

Modern Textile Institute, Donghua University, Shanghai 200051, China
e-mail: yuji@dhu.edu.cn

P. Navard · T. Budtova

MINES ParisTech, PSL Research University, CEMEF - Centre de Mise en Forme des Matériaux, CNRS UMR 7635, CS 10207 rue Claude Daunesse, 06904 Sophia Antipolis Cedex, France

N-oxide monohydrate (NMMO) using the dry-jet wet spinning method with precipitation of fibers in water, alcohol or aqueous NMMO solution bath (Fink et al. 2001). Fibers originated from Lyocell technology are superior to viscose fibers as the former exhibits better tensile properties, a circular cross-section and denser structure with higher crystallinity. However, several problems still remain in Lyocell route such as fiber fibrillation (Ducos et al. 2006) and process instability due to side reactions and byproducts (Rosenau et al. 2001). Thus there is a growing interest in implementing novel and environmentally friendly processes for low cost production of regenerated cellulose fibers.

Recently, alkali-based solvent systems were developed to fabricate regenerated cellulose fibers on laboratory and pilot scale, showing potential in substituting the traditional viscose route. Comprehensive studies of the influence of various spinning parameters, presence of additives in the dope solution (urea, thiourea, ZnO), type of coagulant, coagulation temperature and drawing ratio, on the structure and properties of fibers were performed (Cai and Zhang 2005; Zhang et al. 2002, 2005, 2010a, b). The as-prepared cellulose fibers possess a relatively homogenous structure with high crystallinity. However, the mechanical properties of these novel fibers are not good enough for industrial applications, limited by the low degree of polymerization (*DP*) of cellulose pulps used and the low concentration of spinning solutions. These cellulose solutions are also gelling with time and temperature despite the presence of additives (Cai and Zhang 2006; Liu et al. 2011; Roy et al. 2003; Ruan et al. 2008).

In the laboratory of Donghua University, hydroxyethyl cellulose (HEC) with low molar substitution (*MS*) was prepared by reaction of ethylene oxide (EO) with alkali-cellulose in a heterogeneous process. The solubility of polymer in alkali solvent was significantly improved with the introduction of hydrophilic hydroxyethyl groups. HEC products (membrane or fiber) could be easily available after coagulation of HEC from solutions. These HEC products with *MS* values of 0.30–1.0 presented excellent water related properties compared with other cellulose products, and water retention was improved with the increasing *MS* value (Li et al. 2014), showing that HEC products have enormous application potentials in medical field as water absorbent materials. The HEC products with *MS* values of 0.17–0.3, which had moderate water

related properties, can be used in textiles similar to viscose fibers. In our previous study, HEC fibers were prepared via wet spinning from 9 wt% HEC solution of 0.30 *MS* in the complex solvent composed of 8 wt% NaOH/8 wt% urea/6.5 wt% thiourea (Wang et al. 2013). The resultant fibers have excellent physical properties which should satisfy commercial requirements. However, the addition of urea or thiourea as stabilizers against gelation imposes extra burdens on the recycling and disposal of chemicals in the industrial production. It would be better if NaOH aqueous solution without additives is used to dissolve cellulose or its derivatives because of the cheapness and abundant source of supply of this solvent.

The performance of wet-spun cellulose fibers is governed by their supramolecular structure and morphological characteristics including crystallinity, crystal sizes, chain orientation, pore sizes and cross-sectional shapes (Jiang et al. 2012b; Um et al. 2004a, b). Those structural features are mainly formed (and can be improved) during the coagulation and drawing process, which are influenced by various factors such as polymer concentration in the spinning solution, polymer molecular weight and molecular weight distribution, composition and temperature of coagulation bath, and drawing ratio (Walczak 2002; Woodings 2001). The drawing step is one of the most important steps that determine the quality of resultant fibers.

In this study, we adopted 8 wt% NaOH aqueous solution to dissolve low substituted HEC at -6°C , and the corresponding HEC fibers were successfully prepared by wet spinning. The effects of drawing parameters on fiber morphologies, crystallinity, molecular chain orientation and tensile properties were investigated in details providing a fundamental support for the production of the novel cellulose fibers.

Experimental

Materials

Cotton linters were purchased from Xiangtai Corporation (Hubei Province, China) with *DP* of 1000 as provided by the manufacturer. EO, NaOH and glacial acetic acid supplied by Enterprise group chemical reagent Co., Ltd were analytical reagents and used without further purification. Reactor and disintegrator were custom-made.

Preparation of HEC

The details on HEC synthesis are given in Wang et al. (2013). Briefly, cellulose was immersed in 21 wt% NaOH aqueous solution under vigorous stirring for 1 h at ambient temperature. Extra NaOH solution was removed and the resultant alkaline cellulose, together with a certain amount of liquid EO, was placed under vacuum in a homemade 2 L stainless steel autoclave. The mixture was stirred at 40 °C for about 100 min until the pressure inside the autoclave dropped to the initial value. The product was then neutralized with acetic acid, repeatedly rinsed with distilled water, and then dried under vacuum. The mass ratio of EO to cellulose was kept at 13:100, and their corresponding *MS* value was about 0.24 as shown in Wang et al. (2013).

Formation of HEC fibers

A certain amount of dried HEC was immersed into the 8 wt% NaOH aqueous solution pre-cooled to –6 °C. Transparent HEC solutions with different concentrations were obtained after vigorous stirring for about 2 h. Then the resultant HEC solutions were subjected to centrifugation at 5,000 rpm for 20 min in order to remove the air bubbles, and then kept in refrigerator in closed vessels before use.

The pilot scale wet-spinning apparatus as shown in Fig. 1 was used to manufacture HEC fibers. 6 wt% HEC solution was transferred to the vacuumed spinning tank under N₂ pressure through a candlewick filter with polypropylene (PP) filter fabric (twill; weight: 200 g/m²; air permeability: 145.7 L/m² s). The spinning solution stayed in the vacuum tank for at least 6 h at 30 °C to remove bubbles. A pressure of 0.2–0.3 MPa was applied to extrude the spinning solution through a

spinneret with 200 orifices (0.08 mm in diameter). A metering pump (0.835 mL/rpm) was used for precisely controlling the volume of the spinning solution extruded. Another candlewick filter with PP fabric was placed between the spinning tank and spinneret. Besides, two layers of PP fabrics were placed inside the spinneret before extrusion for further filtration. The spinneret cylinder was immersed in the coagulation bath composed of 10 wt% H₂SO₄/20 wt% Na₂SO₄/1.25 wt% ZnSO₄ at 30 °C under different jet stretches. The fibers subsequently entered the circulating water bath at 95 °C, and further drawing-up was done. The fibers collected from the take-up device were washed with flowing deionized water until the pH of water was equal to 7. Finally, the fibers were gradually dried in the air.

The jet stretch ratio is defined as the ratio of the first stretch roller velocity to the dope extrusion velocity. Similarly, the post-drawing ratio is defined as the ratio of velocities of two stretching rollers. The jet stretch ratios and the post-drawing ratios can be tuned by changing the speed of the first or second stretch roller, respectively. The resultant fibers were named as F-1_M, F-2, F-3_M, F-4, F-5, F-6, F-7_M, where the subscript M stands for the maximum post-drawing ratio that as-spun fibers can sustain without breakage at a fixed jet stretch ratio. The corresponding drawing conditions are shown in Table 1. Note that in this study jet stretch ratio less than one is selected to fabricate the novel fibers, because the HEC stream after extrusion is in a viscous state and could not suffer from too strong tension.

Rheological measurements

The steady and dynamic rheology of HEC solution was investigated using a Bohlin Gemini rheometer

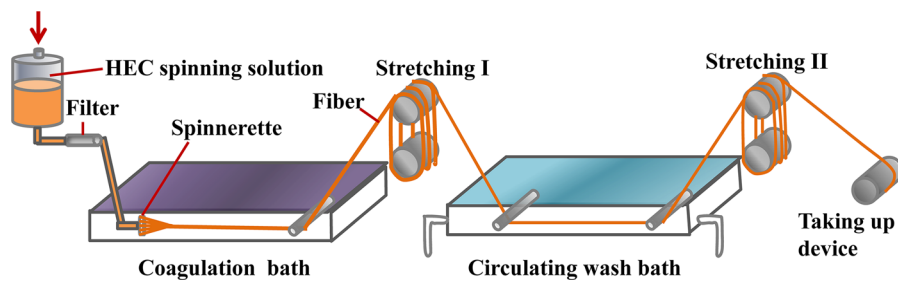


Fig. 1 Scheme of the spinning device

Table 1 The structural features and tensile properties of HEC fibers

Drawing process	F-1 _M	F-2	F-3 _M	F-4	F-5	F-6	F-7 _M
Jet stretch ratio	0.60	0.47	0.47	0.31	0.31	0.31	0.31
Post-drawing ratio	1.8	1.8	1.9	1.8	1.9	2.1	2.2
Fiber diameter (μm)	18.8	21.3	20.9	26.8	25.8	25.7	25.1
Tensile strength (cN/dtex)							
Dry	1.81	1.78	1.85	1.73	1.83	1.96	2.12
Wet	0.60	0.54	0.62	0.50	0.59	0.71	0.85
Elongation at break (%)							
Dry	13.8	15.1	14.5	15.5	14.7	13.1	12.7
Wet	17.2	19.7	18.6	21.4	18.7	17.3	16.4
Crystallinity (%)	52.1	49.2	50.0	48.8	50.5	54.5	55.2
Crystallite orientation f_c	0.82	0.82	0.83	0.78	0.82	0.84	0.84
Sonic orientation f	0.78	0.71	0.77	0.64	0.72	0.84	0.89
R_1 (Å)	29.9	29.0	26.9	28.1	28.5	24.1	22.4
R_2 (Å)	85.8	77.1	75.4	82.7	79.3	76.9	73.4
R_3 (Å)	167.3	158.3	149.6	153.2	144.4	143.1	141.1
Microvoid length L (nm)	320	320	330	310	350	370	390
Misorientation B_ϕ (°)	13.86	15.17	11.54	16.94	11.99	11.04	10.90

with a Peltier temperature control system and cone-plate geometry (cone angle 2°, plate diameter 60 mm). Silicone oil (DC 200, Sigma-Aldrich) spread at the edge of gap together with a solvent trap was used to prevent water evaporation.

The steady-state viscosity of HEC solutions with various concentrations was measured at shear rates between 0.1 and 100 s⁻¹ at 30 °C. The dynamic rheological measurements were conducted at the stress of 0.1 Pa and the frequency of 1 Hz to guarantee the solution being in linear viscoelastic regime. Gelation time t_{gel} of 6 wt% HEC solution at 30 °C was determined from the time evolution of the elastic G' and viscous G'' moduli at the moment when $G' = G''$.

Synchrotron X-ray measurements

HEC fibers prepared at different drawing conditions were investigated by synchrotron wide-angle X-ray diffraction (WAXD) and small-angle X-ray scattering (SAXS) measurements, which were carried out at 16B1 Beamline station in Shanghai synchrotron radiation facility (SSRF) with a wavelength of 0.124 nm. The distance between the sample and CCD detector (MAR CCD-165) was 115 mm for WAXD and 2,075 mm for SAXS, and a typical image acquisition time was 30 s. After being corrected for

the air scattering, the 2D diffraction patterns were transferred with software FIT2D into 1D integrated intensity profiles.

Crystallinity of samples was determined from the integrated diffraction intensity profiles. Individual crystal reflection peak and amorphous background were extracted using curve-fitting method with software Peakfit 4.12. The crystallinity was calculated as the ratio of the total crystal peak intensity to the total diffraction intensity.

The crystal orientation parameters of HEC fibers were evaluated from 2D WAXD images. The azimuthal intensity distribution along the distinctive overlapping (110)/(020) reflections, which was at an angle of 90° with respect to the crystallographic *c*-axis of the cellulose crystal, was analyzed to monitor the total crystal orientation variation, as outlined by Ruan et al. (2006). The dependence of diffraction intensity on the azimuthal angle was fitted with a Gaussian function. Equation 1 (Yamane et al. 1996) was used to calculate the degree of orientation (f_c):

$$f_c = (180 - H)/180 \times 100 \% \quad (1)$$

where H is the full width at half maximum intensity ($FWHM$) of the azimuthal scan curve corresponding to (110)/(020) planes.

The SAXS patterns for HEC fibers show a streak along the equator, which could be interpreted as the

scattering from microvoids generated during the phase separation process according to previous researches (Crawshaw and Cameron 2000; Heikens 1959; Schurz et al. 1995; Statton 1956). These microvoids may be elongated when the wet-spun fibers are subjected to tension during the drawing process, since the processing parameters influence the size, length and orientation of microvoids.

Assuming that the novel fibers contain microvoids with several size levels, the X-ray scattering intensity can be simply expressed in the following Eq. 2 on the basis of Guinier approximation:

$$I(q) = I_e N_1 n_1^2 e^{-q^2 R_{g1}^2/3} + I_e N_2 n_2^2 e^{-q^2 R_{g2}^2/3} + \dots + I_e N_i n_i^2 e^{-q^2 R_{gi}^2/3} \quad (2)$$

where q stands for the scattering vector defined as $q = 4\pi \sin\theta/\lambda$, λ is wavelength, θ is scattering angle; i represents the i th size level. N_i and n_i are, respectively, the void number and the electron number of the voids with gyration radius R_{gi} ; I_e is the scattering intensity of one electron.

A successive tangent method based on Guinier approximation was applied to decompose the contributions of microvoids with different sizes (Fischer et al. 1978; Jellinek et al. 1946). $-R_{gi}^2/3$ could be obtained from the slope of the i th tangent. As the microvoids in the cellulose fibers are usually regarded to be of needle shape with circular cross-section (Jiang et al. 2012a; Moss et al. 2002), the relationship between the average radius R of the microvoids in cross-section and the gyration radius R_g can be described as follows (Guinier et al. 1955; Jiang et al. 2012a):

$$R_i = \frac{5}{3} R_{gi}^2 \quad (3)$$

The radii of microvoids at different levels can be determined for each sample from the slopes of corresponding tangents. Besides, the average microvoids length (L) and misorientation (B_{obs}) of microvoids can also be determined from the SAXS images according to Ruland method (1969).

Sonic measurements

Sonic measurements were performed with a pulse propagation meter to estimate the overall orientation in the prepared fibers. A single filament with 0.1 cN/dtex

tensile stress was mounted between two transducers containing a piezoelectric ceramic crystal with a natural frequency of 5 kHz. Pulses of sonic energy were sent from one bimorph down the filament to the receiving bimorph, and the transmission time was recorded. The sound velocity was computed from the transmission time of the sonic pulse and the distance between the bimorphs. In the case of partially oriented polymer molecules, an angle φ exists between the direction of sound propagation and the molecular axis, which is also the orientation angle of molecular axis along the fiber axis. According to Moseley's report (1960), the relationship between φ and sound velocity along the fiber axis is given by Eq. 4:

$$\overline{\cos^2 \varphi} = 1 - \frac{2}{3} \cdot \frac{C_u^2}{C^2} \quad (4)$$

where C_u and C stand for the sonic velocity in a randomly oriented and uniaxially oriented fiber, respectively. The orientation factor f is defined in Eq. 5:

$$f = \frac{3 < \cos^2 \varphi > - 1}{2} = 1 - \frac{C_u^2}{C^2} \quad (5)$$

Scanning electron microscope (SEM) measurements

The morphologies of the novel fibers were studied with SEM (PHILIPS XL30) at the acceleration voltage of 7 kV. The samples were fractured in liquid nitrogen and sputtered with gold.

Tensile tests

The linear density of a fiber was measured with a XD-1 fiber fineness machine, and tensile tester XQ-1 was used to study the tensile properties of the novel fibers (both XD-1 and XQ-1 were made at Donghua University, Shanghai, China). The gauge length was 20 mm and tensile speed was 5 mm/min. The results were the average values from 30 trials for each specimen. These data were acquired at 20 °C and 65 % relative humidity.

Results and discussion

Rheological properties of HEC solutions

It is well known that the rheological properties of spinning solution exert significant impact on the

shaping process, structure formation, and properties of fibers prepared by wet spinning. Figure 2a describes the steady-state viscosity of HEC solutions of various concentrations as a function of shear rate at 30 °C. At low shear rates, the flow was Newtonian, and then shear thinning occurred above a certain shear rate. The typical shear-thinning behavior results from the stretching and orientation of HEC chains. With the increase of HEC solution concentration, the shear viscosity classically increased and the shear thinning behavior happened at lower shear rates. In this article, considering the flowability of the spinning solution as well as filtration and degassing processes, 6 wt% HEC solution with moderate viscosity was used to prepare fibers.

Figure 2b depicts the evolution of G' and G'' of the 6 wt% HEC solution with time at 30 °C in order to investigate the solution stability. HEC solution remained more or less stable during the first 8 h demonstrating slight variation of η^* , G'' and G' with time. Above 13–14 h, the G' values increased sharply due to the beginning of gelation. In about 18 h, gelation occurred. Subsequently, G' kept on increasing without showing a plateau, indicating that the solution exhibited elastic behavior but hardly reached its equilibrium state. As compared with a 6 wt% micro-crystalline cellulose (MCC)/8 wt% NaOH solution stabilized with 1.5 wt% ZnO at 30 °C which was gelling in about 2.5 h (Liu et al. 2011), the 6 wt% HEC solution exhibited excellent stability beneficial to continuous spinning. It is worth mentioning that

unlike cellulose/NaOH/water systems (Roy et al. 2003; Weng et al. 2004), the HEC solution after the gel point was still flowing instead of transforming into a solid gel, suggesting that the gel formed in HEC solution is much weaker and can be easily broken by a small shear force. The excellent stability towards gelation of HEC solutions can be interpreted by the presence of ether groups, which prevent the formation of hydrogen bonds between cellulose chains because of the geometrical constraints.

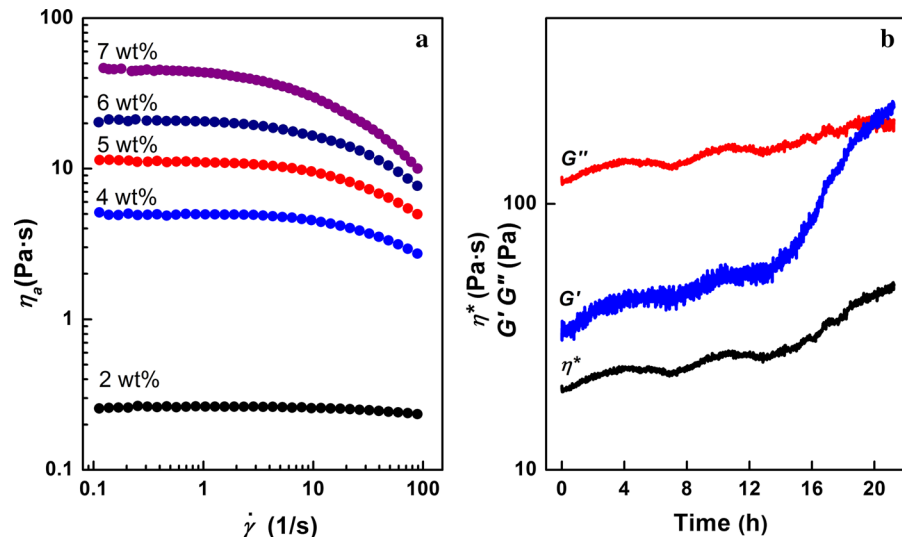
Influence of drawing on the structure and properties of HEC fibers

Stretching is an important processing step in the wet spinning which affects the formation of fiber structure by parallel orientation of chains. Stretching must be imposed on the as-spun fibers during or very soon after extrusion to achieve tensile properties acceptable for textile end-uses. The influence of jet stretch and post-drawing ratios on the morphology, crystallinity, crystal orientation, microvoid characteristics and tensile properties of HEC fibers are presented in Table 1 and discussed below.

Crystal structure and molecular orientation

Figure 3a displays the 2D WAXD patterns of HEC fibers prepared under different drawing conditions and the corresponding 1D integrated profile taken for F-7_M sample is shown in Fig. 3b. HEC fibers displayed

Fig. 2 Steady-state viscosity (η_a) as a function of shear rate for HEC solutions with different concentrations at 30 °C (a); storage modulus G' , loss modulus G'' and complex viscosity η^* of a 6 wt% HEC solution as a function of time at a frequency of 1 Hz (b)



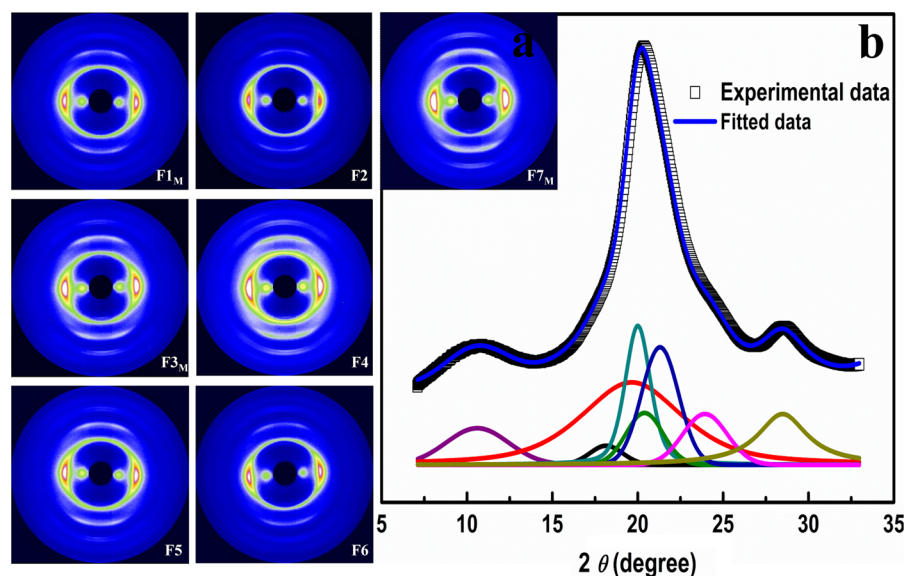
crystal structure similar to typical cellulose II with the characteristic reflections ($\bar{1}10$), (110) and (020) on the equator. The 2D patterns from F-1_M to F-7_M fibers exhibited diffraction arcs with slightly differences in length and intensity, reflecting variations in crystal orientation and crystallinity. Integrated WAXD profile showed that ($\bar{1}10$), (110) and (020) reflections were located at around 10.8, 20.5 and 21.4°, respectively. The transition from cellulose I into cellulose II occurred after cellulose was immersed in 21 wt% NaOH solution. The following etherification slightly changed the cellulose II crystal structure because of the introduced hydroxyethyl groups, which was confirmed in our previous study (Li et al. 2014). The peaks of plane (020) were merged into the peaks of plane (110), while the peak of ($\bar{1}10$) was shifted to a lower angle (10.8°) compared with 12° of cellulose II (Langan et al. 2005) due to the increased inter-planar distance of plane ($\bar{1}10$).

The crystal structure of HEC fibers is primarily formed during the coagulation process, closely related to the jet stretch. As shown in Table 1, when the post-drawing ratio was fixed at 1.81, the rising in jet stretch ratio increased the crystallinity of HEC fibers from 48.8 to 52.1 %, indicating that orientation-induced crystallization occurred with stretching. Meanwhile the crystal orientation of fibers increased slightly from 0.78 to 0.82, and then seemed to stay constant. This indicates that the molecular chains are straightened out with higher jet stretch ratio, thus increasing the ease to

form crystalline entities. However, it was difficult to increase the crystal orientation in the fiber direction above a certain value mostly due to steric hindrance. In spite of the saturation of the crystalline phase orientation, more and more chains in amorphous regions continued to be oriented along the fiber axis when the jet stretch ratio increased, which can be confirmed by the rising of the overall orientation of HEC fibers (changing from 0.64 to 0.78 with the increasing jet stretch ratio as shown in Table 1). The increased chain mobility and the fact that entangled chains are trapped between crystals could explain in part this increase of amorphous chain orientation.

The supramolecular structure of HEC fibers was further improved when the as-spun fibers were stretched during the following treatment in hot water bath. As the post-drawing ratio increased from 1.8 to 2.2 with jet ratio fixed at 0.31, the crystallinity, crystal orientation together with the sonic orientation went up distinctively. The reason for the increasing crystallinity could be explained as follows. As the jet stretch ratio applied in this study was relatively low, the chains of as-spun fibers after coagulation were in a loose arrangement due to lack of effective drawing. When the fibers were subjected to the tension of post-drawing, the chains were stretched along the fiber axis and the distance between the adjacent HEC chains was decreased, leading to the improvement in the structural regularity of fibers and a significant increase in crystallinity. If higher jet stretch ratio was used, the

Fig. 3 2D WAXD patterns of HEC fibers under different drawing conditions (a), and integrated intensity profile of F-7_M fibers (b). The corresponding peak deconvolution was used for calculating the crystallinity



arrangement of HEC chains after coagulation would be much more compact. The influence of following post-drawing on the crystal structure of HEC fibers would be weakened, as shown in the case of F-2 and F-3_M fibers. Interestingly, F-3_M fibers prepared at the maximal post-drawing ratio with 0.47 jet ratio, possessed lower crystallinity and less oriented structure than F-7_M fibers with 0.31 jet ratio (Table 1), implying that it is the post-drawing process that is playing the key role in the formation of supramolecular structure.

Generally, three different deformation mechanisms are involved in the jet stretch and post-drawing process (Gupta and Kothari 1997). The first one is the viscous flow deformation, during which macromolecules are in a viscoelastic state with a high relaxation rate. Orientation is difficult to be kept due to chain conformation relaxation. In the following step the elastic deformation starts to work. The macromolecules begin to orient under the external drawing forces. However, this orientation effect could remain owing to the recoverable elastic strain after the removal of external force. Elastic deformation is also bringing internal stresses into the fibers, which deteriorate the structure and properties. The third deformation mechanism has a plastic character, which allows permanently retaining the oriented structure of fibers caused by external force. When the stress is applied, the chains slide one over another and the interactions between them induce a new organization during which new elongated conformation of macromolecules is produced and kept, resulting in a non-recoverable plastic deformation. The viscous flow deformations are mainly acting in the jet stretch, while most of the plastic deformation occurs during the post-drawing process. That is why the post-drawing process has more significant influences on the supramolecular structure of HEC fibers.

Microvoid morphology of HEC fibers spun under different drawing conditions

Apart from the supramolecular chain structure, the porous structure of HEC fibers also influences fiber properties. The microvoids in HEC fibers are formed during coagulation as a result of phase separation accompanied by volume change. Stretching process changes the size, length and orientation of these voids. We used SAXS to analyze the microvoids in fibers, in

the same way as it was done by other authors (Crawshaw and Cameron 2000; Kaburagi et al. 2003; Ran et al. 2001; Schurz et al. 1995). Figure 4 shows the 2D SAXS patterns of HEC fibers prepared at different drawing ratios. The patterns showed sharp and elongated streak along the equator as well as relatively weak and short meridian streak. The appearance of the equatorial scattering in SAXS patterns was supposed to be mainly associated with the long and narrow voids oriented preferably along fiber axis, while meridian streak was attributed to the increased misorientation of the voids and a reduction in void length (Ruland 1969).

Figure 5 shows an example of the Guinier plots of equator scattering intensities and the tangent curves for F-7_M fibers. The radii of microvoids in the cross-section of HEC fibers were calculated from the slopes of tangent lines and the results are presented in Table 1. SAXS results were also used to obtain azimuthal scans taken at different s ($s = q/2\pi = 2 \sin\theta/\lambda$). Figure 6a shows the azimuthal scans of F-7_M fibers and the corresponding Ruland plot is illustrated in Fig. 6b. The resulting azimuths of equatorial scattering streaks were fitted using a Gaussian distribution (Eq. 6) with standard deviation R^2 of around 0.995:

$$(s \cdot B_{obs})^2 = \left(\frac{1}{L}\right)^2 + (s \cdot B_\phi)^2 \quad (6)$$

where B_{obs} is the full width at half maximum of the azimuthal profile from the equatorial streak fitted with a Gaussian function; L is the average length of microvoids and B_ϕ represents the width of the orientation distribution of the voids. Ruland plot (Fig. 6b) was used to calculate B_ϕ as the slope and L as the intercept of $(s \cdot B_{obs})^2$ versus s^2 .

All three levels of diameters of voids in the cross-section decreased from F-4 to F-7_M fibers (Table 1), showing that the rising post-drawing ratio leads to the shrinkage in cross-section of microvoids and the increase in their length. However, the increase in jet ratio from 0.31 to 0.60 with a fixed post-drawing ratio of 1.8 produced slightly larger voids. It is supposed that the increase in microvoid sizes was related to the increase of internal stress during coagulation as the stress imposed by stretching was increased and the residence in the coagulation bath was reduced. Furthermore, the misorientation B_ϕ of the microvoids

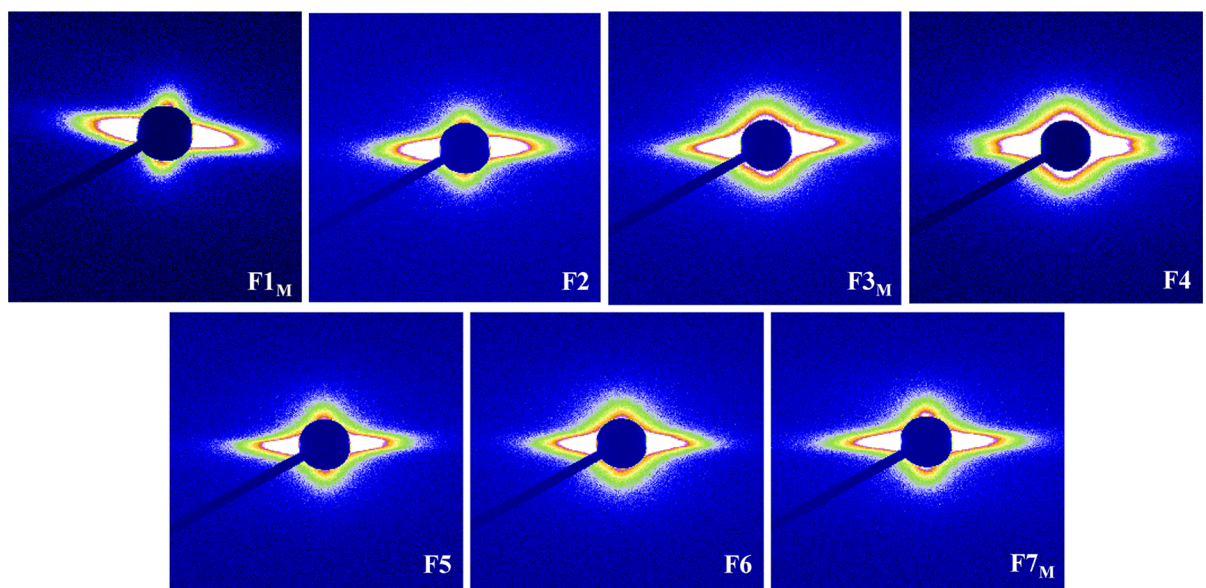


Fig. 4 2D SAXS patterns of HEC fibers under different drawing conditions

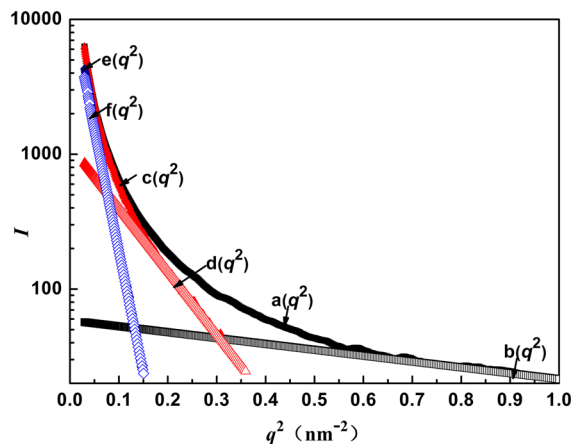


Fig. 5 Guinier plots of the scattered intensity for F-7_M fibers. $a(q^2)$ is the experimental scattering curve. Line $b(q^2)$ is the first tangent at the largest scattering angle of the logarithm plot of $a(q^2)$, allowing to calculate the radius R_1 of microvoids based on the slope of $b(q^2)$. Curve $c(q^2)$ is the intensity difference between $a(q^2)$ and $b(q^2)$ in linear intensity scale. Repeating the above procedure, the second tangent $d(q^2)$ is performed on curve $c(q^2)$. After subtracting $d(q^2)$ from curve $c(q^2)$, the remaining curve $e(q^2)$ could hardly be subtracted by the third tangent $f(q^2)$. The other two levels of microvoid diameters R_2 , R_3 were determined by the slope of corresponding tangents $d(q^2)$ and $f(q^2)$, respectively

was reduced with the increasing jet ratio and post-drawing ratio, which is consistent with the results of crystal orientation.

Morphologies of HEC fibers

Even though prepared at different drawing conditions, HEC fibers exhibited similar longitudinal shapes with relatively smooth surface, and longitudinal shape of F-7_M fibers as an example is illustrated in Fig. 7a. Figure 7b–h shows the SEM images of the cross-sections of the wet-spun HEC fibers prepared under different drawing conditions. At a constant post-drawing ratio of 1.8, the increase of jet stretch ratio from 0.31 to 0.60 induced the decrease of the average diameter of HEC fibers, whereas the increase in post-drawing ratio at a constant jet stretch ratio just slightly modified fiber diameter from 26.8 μm for F-4 fibers to 25.1 μm for F-7_M fibers. Therefore, thinner fibers can be developed through increasing the jet stretch ratio.

Furthermore, all HEC fibers exhibited oval or circular cross-sections with a thin surface layer. A layer close to the surface (usually called sub-layer) shows large, elongated voids running in the radial direction. The origin of this phenomenon is well known in membrane science where membranes prepared by immersion of a polymer solution in coagulation bath under delayed precipitation conditions display such cell structures. A large body of work has been published to explain the formation of such structures through the nucleation and growth of a polymer poor phase. A review of the mechanisms

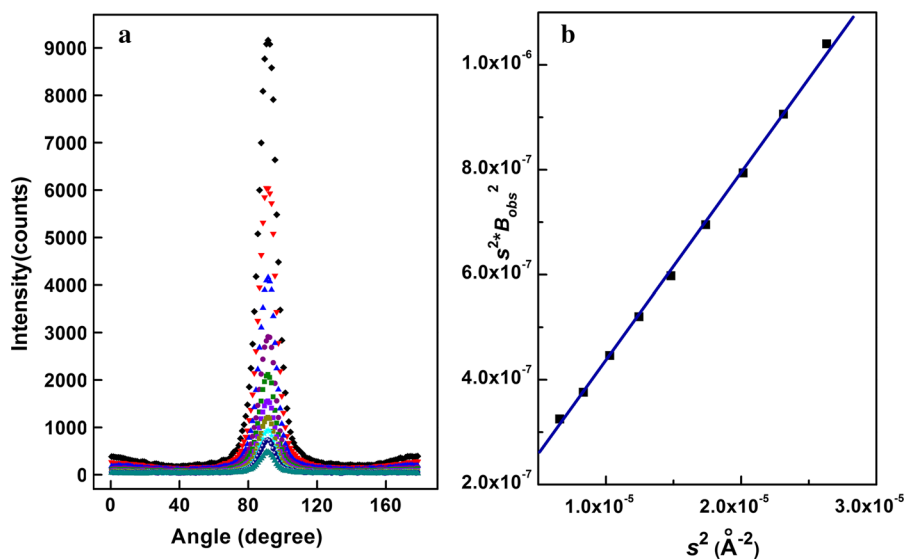


Fig. 6 Azimuthal scans (**a**) at different s values for F-7_M fibers in Fig. 3b and the corresponding Ruland plot (**b**)

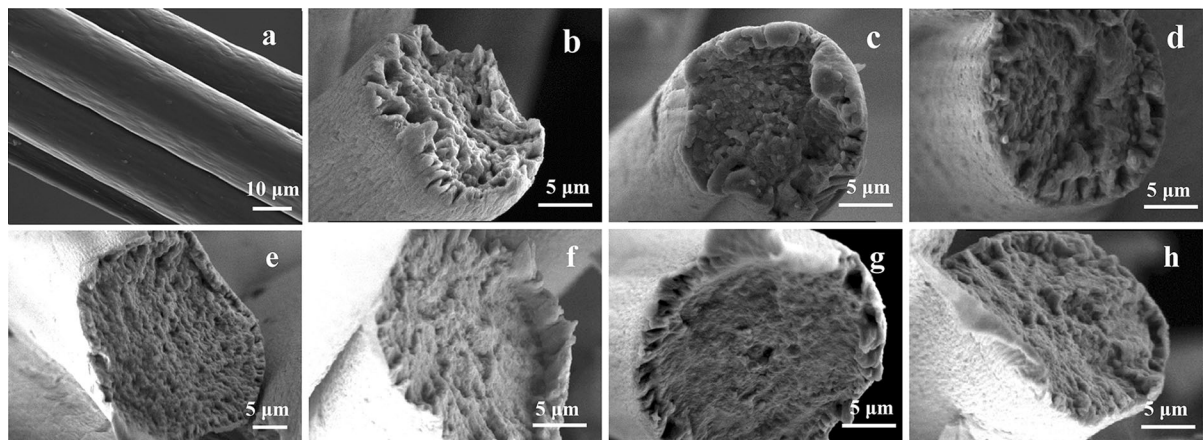


Fig. 7 SEM photographs of longitudinal shape of F-7_M fibers (**a**), and (**b–h**) cross-sections of HEC fibers from F-1_M to F-7_M

involved during the formation of polymeric membranes by phase separation in a polymer solution was published by Van de Witte et al. (1996). The cross-sectional shape of wet spun fibers is closely related with the phase separation processes (Liu et al. 1989). A relatively gentle solidification condition (coagulation temperature was 30 °C, lower than that of viscose route) together with a spinning solution prepared from the polymer with high DP, would decrease the mass transfer rate difference between solvent and coagulants, thus favoring the creation of sub-layered pores, leading to a soft, deformable coagulated layer. Unlike the viscose fibers with a rigid skin, a circular cross-

sectional shape was formed due to such soft and deformable surface layer. However, it is possible that the property of surface layer would also lead to small deviations of the cross-sections from circularity when the fibers were subjected to compression during the drawing or drying process. Except the outer layer, the morphologies of cross-sections of F-1_M, F-2 and F-3_M fibers spun with higher jet stretch ratio were relatively rough and loose, while the other four HEC fibers spun with the lowest jet stretch ratio exhibited uniform and dense features. When the lower jet stretch ratio was used, the as-spun fibers under reduced tension spent more time in the coagulation bath due to the decrease

of spinning speed. Thus there was sufficient time for HEC macromolecules to relax during the fiber formation, resulting in fibers with lower internal stresses and more uniform structure.

Tensile properties of HEC fibers

Table 1 summarizes the tensile properties of HEC fibers spun under different drawing conditions. At the lowest jet stretch and post-drawing ratios, 1.73 cN/dtex of tenacity as well as 15.5 % of elongation at break were endowed for F-4 fibers. As the jet stretch ratio increased, the tenacity slightly increased to 1.81 cN/dtex accompanied with 13.8 % of elongation at break (F-1_M fibers), while the increase of post-drawing ratio induced about 20 % increase in fiber tenacity and similar decrease in the elongation at break. F-7_M fibers spun at the highest drawing ratio had the highest tenacity of 2.12 cN/dtex and 12.7 % elongation at break, close to those of common viscose fibers and fibers from cellulose-NaOH-urea aqueous solutions, which exhibited tenacity around 2.0–2.4 and 1.63–1.97 cN/dtex, respectively (Li et al. 2010). It is worth noting that lower jet stretch ratio leaves more potential space for as-spun fibers to be further stretched during the post-drawing process. Therefore, the HEC fibers prepared at higher post-drawing ratio generally have better tensile properties.

It must be mentioned here that the tensile strength of the wet HEC fibers is a bit lower than that of commercial rayon fibers with wet tenacity of about 1.0 cN/dtex. The introduction of hydrophilic hydroxyethyl groups increases the distances between HEC chains as well as fiber hydrophilicity which causes swelling, and thus weakens their tensile properties in wet state. The tensile properties of wet HEC fibers still have the potential to be improved by finding the best compromises between molar substitution which controls polymer solubility, solution stability and fiber tensile properties. Another useful method is “sealing off” the free hydroxyl groups of HEC by crosslinking reactions during the spinning process, as what has been done for collagen fibers (Zeugolis et al. 2009).

Conclusions

HEC fibers were prepared by wet spinning from low-substituted HEC dissolved in 8 wt% NaOH aqueous

solution. This system had a higher stability in terms of gelation time as compared to microcrystalline cellulose in similar alkali solvents. Fiber structure, morphologies and tensile properties were investigated as a function of spinning parameters such as jet stretch and post-drawing ratios. The HEC fibers displayed oval or circular cross-sections with a porous outer layer and a dense core. The crystallinity, crystal orientation, sonic orientation as well as microvoid orientation in the fibers were improved with increasing jet stretch and post-drawing ratios, whereas the microvoid length slightly decreased with the jet stretch, but distinctively increased with the post-drawing. The HEC fibers prepared at relatively low jet stretch ratio and high post-drawing ratio presented the best tensile properties, indicating that post-drawing process is the key step in tailoring the fiber structure as well as tensile properties due to the plastic deformation under drawing.

Acknowledgments This work has been financially supported by the Fundamental Research Funds for the Central Universities, WAXD and SAXS experiments were performed at 16B1 Beamline station in Shanghai Synchrotron Radiation Facility (SSRF). Authors are grateful to Suzanne Jacomet (CEMEF, Mines ParisTech) for help in SEM observations.

References

- Cai J, Zhang L (2005) Rapid dissolution of cellulose in LiOH/urea and NaOH/urea aqueous solutions. *Macromol Biosci* 5:539–548. doi:[10.1002/mabi.200400222](https://doi.org/10.1002/mabi.200400222)
- Cai J, Zhang L (2006) Unique gelation behavior of cellulose in NaOH/urea aqueous solution. *Biomacromolecules* 7:183–189. doi:[10.1021/bm0505585](https://doi.org/10.1021/bm0505585)
- Crawshaw J, Cameron R (2000) A small angle X-ray scattering study of pore structure in Tencel cellulose fibres and the effects of physical treatments. *Polymer* 41:4691–4698. doi:[10.1016/S0032-3861\(99\)00502-9](https://doi.org/10.1016/S0032-3861(99)00502-9)
- Ducos F, Biganska O, Christian Schuster K, Navard P (2006) Influence of the Lyocell fibers structure on their fibrillation. *Cell Chem Technol* 40:299–311
- Fink H, Weigel P, Purz H, Ganster J (2001) Structure formation of regenerated cellulose materials from NMMO-solutions. *Prog Polym Sci* 26:1473–1524. doi:[10.1016/S0079-6700\(01\)00025-9](https://doi.org/10.1016/S0079-6700(01)00025-9)
- Fischer E, Herchenröder P, Manley R, Stamm M (1978) Small-angle neutron scattering of selectively deuterated cellulose. *Macromolecules* 11:213–217. doi:[10.1021/ma60061a039](https://doi.org/10.1021/ma60061a039)
- Guinier A, Fournet G, Walker CB, Yudowitch KL (1955) Small-angle scattering of X-rays. Wiley, New York
- Gupta V, Kothari V (1997) Manufactured fibre technology. Springer, The Netherlands

- Heikens D (1959) A quantitative investigation on the X-ray small angle scattering of cellulose fibers. Part I. The concept of scattering power and a method for its determination in electron units. *J Polym Sci* 35:139–143. doi:[10.1002/pol.1959.1203512811](https://doi.org/10.1002/pol.1959.1203512811)
- Jellinek M, Solomon E, Fankuchen I (1946) Measurement and analysis of small-angle X-ray scattering. *Ind Eng Chem Anal* 18:172–175. doi:[10.1021/i560151a005](https://doi.org/10.1021/i560151a005)
- Jiang G, Huang W, Li L, Wang X, Pang F, Zhang Y, Wang H (2012a) Structure and properties of regenerated cellulose fibers from different technology processes. *Carbohydr Polym* 87:2012–2018. doi:[10.1016/j.carbpol.2011.10.022](https://doi.org/10.1016/j.carbpol.2011.10.022)
- Jiang G, Yuan Y, Wang B, Yin X, Mukoze K, Huang W, Zhang Y, Wang H (2012b) Analysis of regenerated cellulose fibers with ionic liquids as a solvent as spinning speed is increased. *Cellulose* 19:1075–1083. doi:[10.1007/s10570-012-9716-2](https://doi.org/10.1007/s10570-012-9716-2)
- Kaburagi M, Bin Y, Zhu D, Xu C, Matsuo M (2003) Small angle X-ray scattering from voids within fibers during the stabilization and carbonization stages. *Carbon* 41:915–926. doi:[10.1016/S0008-6223\(02\)00407-4](https://doi.org/10.1016/S0008-6223(02)00407-4)
- Langan P, Sukumar N, Nishiyama Y, Chanzy H (2005) Synchrotron X-ray structures of cellulose I β and regenerated cellulose II at ambient temperature and 100 K. *Cellulose* 12:551–562. doi:[10.1007/s10570-005-9006-3](https://doi.org/10.1007/s10570-005-9006-3)
- Li R et al (2010) Primarily industrialized trial of novel fibers spun from cellulose dope in NaOH/urea aqueous solution. *Ind Eng Chem Res* 49:11380–11384. doi:[10.1021/ie101144h](https://doi.org/10.1021/ie101144h)
- Li F, Wang W, Wang X, Yu J (2014) Changes of structure and property of alkali soluble hydroxyethyl celluloses (HECs) and their regenerated films with the molar substitution. *Carbohydr Polym* 114:206–212. doi:[10.1016/j.carbpol.2014.08.015](https://doi.org/10.1016/j.carbpol.2014.08.015)
- Liu C, Cuculo J, Smith B (1989) Coagulation studies for cellulose in the ammonia/ammonium thiocyanate ($\text{NH}_3/\text{NH}_4\text{SCN}$) direct solvent system. *J Polym Sci B Polym Phys* 27:2493–2511. doi:[10.1002/polb.1989.090271208](https://doi.org/10.1002/polb.1989.090271208)
- Liu W, Budtova T, Navard P (2011) Influence of ZnO on the properties of dilute and semi-dilute cellulose-NaOH-water solutions. *Cellulose* 18:911–920. doi:[10.1007/s10570-011-9552-9](https://doi.org/10.1007/s10570-011-9552-9)
- Moseley WW (1960) The measurement of molecular orientation in fibers by acoustic methods. *J Appl Polym Sci* 3:266–276. doi:[10.1002/app.1960.070030902](https://doi.org/10.1002/app.1960.070030902)
- Moss C, Butler M, Müller M, Cameron R (2002) Microfocus small-angle X-ray scattering investigation of the skin–core microstructure of lyocell cellulose fibers. *J Appl Polym Sci* 83:2799–2816. doi:[10.1002/app.10256](https://doi.org/10.1002/app.10256)
- Philipp B (1993) Organic solvents for cellulose as a biodegradable polymer and their applicability for cellulose spinning and derivatization. *J Macromol Sci Part A* 30:703–714. doi:[10.1080/10601329308021256](https://doi.org/10.1080/10601329308021256)
- Ran S, Zong X, Fang D, Hsiao BS, Chu B, Phillips RA (2001) Structural and morphological studies of isotactic polypropylene fibers during heat/draw deformation by in situ synchrotron SAXS/WAXD. *Macromolecules* 34:2569–2578. doi:[10.1021/ma0016477](https://doi.org/10.1021/ma0016477)
- Rosenau T, Potthast A, Sixta H, Kosma P (2001) The chemistry of side reactions and byproduct formation in the system NMNO/cellulose (Lyocell process). *Prog Polym Sci* 26:1763–1837. doi:[10.1016/S0079-6700\(01\)00023-5](https://doi.org/10.1016/S0079-6700(01)00023-5)
- Roy C, Budtova T, Navard P (2003) Rheological properties and gelation of aqueous cellulose-NaOH solutions. *Biomacromolecules* 4:259–264. doi:[10.1021/bm020100s](https://doi.org/10.1021/bm020100s)
- Ruan D, Zhang L, Lue A, Zhou J, Chen H, Chen X, Chu B, Kondo T (2006) A rapid process for producing cellulose multifilament fibers from a NaOH/thiourea solvent system. *Macromol Rapid Commun* 27:1495–1500. doi:[10.1002/marc.200600232](https://doi.org/10.1002/marc.200600232)
- Ruan D, Lue A, Zhang L (2008) Gelation behaviors of cellulose solution dissolved in aqueous NaOH/thiourea at low temperature. *Polymer* 49:1027–1036. doi:[10.1016/j.polymer.2007.12.044](https://doi.org/10.1016/j.polymer.2007.12.044)
- Ruland W (1969) Small-angle scattering studies on carbonized cellulose fibers. *J Polym Sci Polym Symp* 1:143–151. doi:[10.1002/polc.5070280113](https://doi.org/10.1002/polc.5070280113)
- Schurz J, Lenz J, Wrentschur E (1995) Inner surface and void system of regenerated cellulose fibers. *Die Angewandte Makromolekulare Chemie* 229:175–184. doi:[10.1002/apmc.1995.052290112](https://doi.org/10.1002/apmc.1995.052290112)
- Statton W (1956) Crystallite regularity and void content in cellulose fibers as shown by small-angle x-ray scattering. *J Polym Sci* 22:385–397. doi:[10.1002/pol.1956.1202210204](https://doi.org/10.1002/pol.1956.1202210204)
- Um I, Ki C, Kweon H, Lee K, Ihm D, Park Y (2004a) Wet spinning of silk polymer: II. Effect of drawing on the structural characteristics and properties of filament. *Int J Biol Macromol* 34:107–119. doi:[10.1016/j.ijbiomac.2004.03.011](https://doi.org/10.1016/j.ijbiomac.2004.03.011)
- Um I, Kweon H, Lee K, Ihm D, Lee J, Park Y (2004b) Wet spinning of silk polymer: I. effect of coagulation conditions on the morphological feature of filament. *Int J Biol Macromol* 34:89–105. doi:[10.1016/j.ijbiomac.2004.03.007](https://doi.org/10.1016/j.ijbiomac.2004.03.007)
- Van de Witte P, Dijkstra P, Van den Berg J, Feijen J (1996) Phase separation processes in polymer solutions in relation to membrane formation. *J Membr Sci* 117:1–31. doi:[10.1016/0376-7388\(96\)00088-9](https://doi.org/10.1016/0376-7388(96)00088-9)
- Walczak ZK (2002) Processes of fiber formation. Elsevier, United Kingdom
- Wang W, Zhang P, Zhang S, Li F, Yu J, Lin J (2013) Structure and properties of novel regenerated cellulose fibers prepared in NaOH complex solution. *Carbohydr Polym* 98:1031–1038. doi:[10.1016/j.carbpol.2013.06.076](https://doi.org/10.1016/j.carbpol.2013.06.076)
- Weng L, Zhang L, Ruan D, Shi L, Xu J (2004) Thermal gelation of cellulose in a NaOH/thiourea aqueous solution. *Langmuir* 20:2086–2093. doi:[10.1021/la035995o](https://doi.org/10.1021/la035995o)
- Woodings C (2001) Regenerated cellulose fibres, vol 18. Woodhead Publishing, Cambridge
- Yamane C, Mori M, Saito M, Okajima K (1996) Structures and mechanical properties of cellulose filament spun from cellulose/aqueous NaOH solution system. *Polym J* 28:1039–1047. doi:[10.1295/polymj.28.1039](https://doi.org/10.1295/polymj.28.1039)
- Zeugolis D, Paul G, Attenburrow G (2009) Crosslinking of extruded collagen fibers—a biomimetic three-dimensional scaffold for tissue engineering applications. *J Biomed Mater Res A* 89:895–908. doi:[10.1002/jbm.a.32031](https://doi.org/10.1002/jbm.a.32031)
- Zhang L, Ruan D, Gao S (2002) Dissolution and regeneration of cellulose in NaOH/thiourea aqueous solution. *J Polym Sci B Polym Phys* 40:1521–1529. doi:[10.1002/polb.10215](https://doi.org/10.1002/polb.10215)

- Zhang L, Mao Y, Zhou J, Cai J (2005) Effects of coagulation conditions on the properties of regenerated cellulose films prepared in NaOH/urea aqueous solution. *Ind Eng Chem Res* 44:522–529. doi:[10.1021/ie0491802](https://doi.org/10.1021/ie0491802)
- Zhang S, Li F, Yu J (2010a) Structure and properties of novel cellulose fibres produced from NaOH/PEG-treated cotton linters. *Iran Polym J* 19:949–957
- Zhang S, Li F, Yu J, Hsieh Y (2010b) Dissolution behaviour and solubility of cellulose in NaOH complex solution. *Carbohydr Polym* 81:668–674. doi:[10.1016/j.carbpol.2010.03.029](https://doi.org/10.1016/j.carbpol.2010.03.029)